Quantum Calculation of Ro-vibrational States: Methodology and DOCl Application Results

Hong Zhang, Marlies Hankel, and Sean C. Smith*

Centre for Computational Molecular Science, AIBN Building (#75), The University of Queensland, Qld 4072, Brisbane, Australia

Shinkoh Nanbu

Research Institute for Information Technology, Kyushu University, 6-10-1 Hakozaki, Higashi-ku, Fukuoka 812-8581, Japan

Hiroki Nakamura

Institute for Molecular Science, Myodaiji, Okazaki 444-8585, Japan

Received: January 1, 2008; In Final Form: February 18, 2008

An improved Lanczos eigenvalue analysis method has been developed to compute the bound ro-vibrational states for the DOCl system at a total angular momentum of $J = 0$ and $J = 30$. In this method, the error norm is used to identify all the true eigenvalues, using the Lanczos algorithm without re-orthogonalization. For ro-vibrational spectroscopy calculations, the comparisons among experimental results, the exact quantum mechanical calculations, and the widely used approximate adiabatic rotation method have been made for $J = 30$. For $J = 0$, the density of states (DOS) in both the bound and unimolecular dissociation regime have been computed, whereas for the $J = 30$ case, only the DOS in the lower portion of the bound spectrum has been reported, because of substantial computational tasks.

1. Introduction

Quantum calculations based on iterative methods have become increasingly common recently. These methods are useful especially for large molecular systems, because they do not require explicit storage of the Hamiltonian matrix; rather, they require only multiplication of the Hamiltonian by a vector. When combined with a sparse representation of the Hamiltonian such as a discrete variable representation (DVR),[1] both memory and CPU time can be reduced dramatically. Notably, the Chebyshev and Lanczos iterative methods have been widely applied in both bound and continuum problems.

Lanczos methods exploit the sparcity of the tridiagonal subspace Hamiltonian generated by the iterative Lanczos algorithm.[2] Although the Lanczos algorithm has commonly been used for matrix diagonalization[3] and short-time propagations,[4] recent work in the Brisbane laboratory has focused on exploring more-general applications of the Lanczos representation, including spectral densities,[5−7] filter diagonalization for bound states and resonances,[8−13] partial resonance widths in unimolecular decay,[14] and state-to-state reactive scattering.[15,16] An important feature of these newer Lanczos implementations is that all physically relevant information is extracted from within the Lanczos representation. This allows a single Lanczos iteration of arbitrary length to be utilized for the propagation, rather than a sequence of short iterations. We note that for scattering or resonance applications, the absorbing boundary conditions are imposed within the Lanczos algorithm by incorporation of a complex absorbing potential (CAP) into the Hamiltonian. This has the consequence that the Lanczos iterations are complex and yield a complex-symmetric tridiagonal representation of the Hamiltonian. Significant progress has also been made recently in the search for a real Lanczos subspace method that is capable of computing state-to-state reactive scattering probabilities.[17−19] These new real Lanczos methods require no complex absorbing potential or damping operator.

It is well-known that, because of the loss of orthogonality, the standard Lanczos method encounters the ghosting eigenvalue problem, which is related to the numerical errors in the three-term recursion. There are basically two ways to address this issue. The first approach is to enforce strict orthogonality by explicitly orthogonalizing each new vector against *all* of the previous vectors, at a very high price of memory and speed reduction. The second approach takes advantage of the error analysis of Paige,[20] which demonstrates that the eigenvalues that are duplicated in the presence of ghosting are, nevertheless, accurate. In this latter approach, one simply tolerates the ghosting and designs a means of sorting out the true eigenvalues from the spurious ones. Hence, some care and time is required on the part of the user to determine precisely which are the true eigenvalues. We note that MINRES filter diagonalization,[9] as well as the classic Cullum and Willoughby algorithm,[3] have shown substantial progress for the elimination of the Lanczos ghosting effects. In this paper, our application has demanded the development of a more efficient and accurate approach to identify all the true eigenvalues. The size of the molecular ro-vibational Hamiltonian matrix in this paper is very large ($\sim 10^7 \times 10^7$), and the new algorithm can sensitively identify all of the converged true eigenvalues.

Exact nonzero total angular momentum ($J > 0$) calculations are essential for a complete description of quantum reactive scattering, thermal kinetics, and energy transfer, and also in

* Author to whom correspondence should be addressed. Fax: 61-7-3346-3949. E-mail: s.smith@uq.edu.au.

10.1021/jp8000114 CCC: $40.75
Published on Web 03/27/2008

correctly simulating molecular spectroscopy. This latter application provides the context of the present paper, in which we explore the capabilities of exact quantum dynamical calculation of DOCl rovibrational states for high angular momentum calculations. Experimentally, the high-resolution rotational spectra of the DOCl system have been reported for several vibrational states for J values as high as 50.[21,22] Theoretically, the exact quantum calculation is still a challenging task, especially for the complex-forming systems, wherein the deep potential well and high vibrational excitations demand very large basis sets. Requisite basis sets for the vibrational and bending modes notwithstanding, the major reason for the difficulty is the so-called "angular momentum catastrophe".[23] For these nonzero J calculations, it is apparently impractical to apply conventional direct diagonalization methods, because of the requirement of a large and often-prohibitive computer core memory. Several sophisticated basis set contraction schemes[24,25] do exist, but, because of their unfavorable scaling, they are limited to optimized basis sets of $N < 10000$. Variational approaches can be used to compute the lower bound states accurately; however, for high-lying bound states, convergence becomes difficult as the size of the basis set increases.[26,27] On the other hand, quantum iterative methods such as the Lanczos method[2,3] are well-suited to solving this large-scale eigenvalue problem.

The related HOCl system has been extensively studied from both experimental and theoretical perspectives, because of its importance in atmospheric chemistry.[28−36] It is considered to be a temporary reservoir of the Cl atoms and has been detected by far-infrared emission techniques.[28] For this reason, much effort has been devoted to the spectroscopic study of HOCl in the microwave, far-infrared, and infrared regions of its spectrum. For example, the high-resolution far-infrared spectrum of HOCl has been reported for total angular momentum above 50 with $K_a > 6$.[29,30] However, even this seemingly simple system, which involves only three atoms, turns out to be very difficult to model quantum mechanically for high J values. So far, most of the calculations have focused on the $J = 0$ case, because of obvious computational difficulties. Exact quantum calculations, including Coriolis coupling have been reported only for $J = 1$ and $J = 3$.[34,35] The potential energy surfaces (PESs) mostly used are those by Bowman et al.,[37,38] and those by Schinke et al.[39] These high-quality ab initio PESs are scaled to achieve agreement with the extant spectroscopic data for $J = 0$. Recently, a new global ab initio PES for a HOCl system that is suitable for both spectroscopy and reaction dynamics investigations has been developed by Nanbu et al.[40] The newer ab initio surface by Nanbu et al.[40] is not scaled or adjusted to reproduce the available spectroscopic data. Using this PES, we recently provided the first extensive rigorous calculations for large values of the total angular momentum ranging up to 30.[41] However, in comparison with previous calculations and experimental spectroscopic data at $J = 0$ for a HOCl system, we found that this ab initio PES does not generate the vibrational state energies as accurately as the fitted ab initio PESs. Consequent to this work, substantial ab initio data points have been additionally computed and added to generate an improved version of the Nanbu PES is produced. In this paper, we used this augmented PES to calculate the DOCl ro-vibrational spectroscopy through parallel computing strategy, and some comparisons between the exact calculations and approximate quantum methods such as adiabatic rotation (AR)[42] will be made.

The rest of this article proceeds as follows. In section 2, we describe the theoretical methods needed to characterize ro-vibrational states for nonzero total angular momentum, in particular, the algorithm used to identify all the true eigenvalues in the Lanczos approach. In section 3, we present the results for the $J = 0$ case and 30 calculations performed on the new version of the potential energy surface. Detailed comparisons with previous work for the lower bound-state manifold as well as the comparisons with AR approximation and with experiments will also be given in section 3. The conclusion is given in section 4.

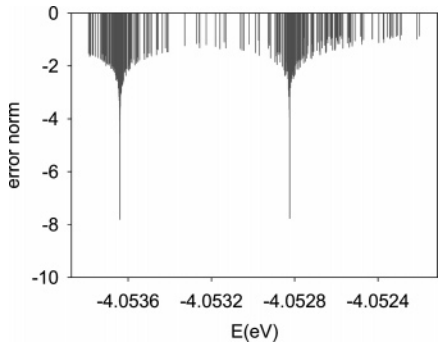

Figure 1. Plot of the logarithmic error norms for the DOCl clustering eigenvalues around the two lowest eigenvalues at $E = -4.053640$ eV and $E = -4.052824$ eV from the $J = 30$ and even symmetry calculations. Here, the ro-vibrational state energy was relative to the $O(^1D) + HCl$ dissociation limit, which is called the zero energy point. The Lanczos subspace size is $M = 150\,000$.

2. Methodology

2.1. Hamiltonian and Representation. Generally, we treat the three internal Jacobi coordinates (R, r, γ) in discrete variable representation (DVR), while the three Eulerian angles (θ, ϕ, ψ) are described in a basis set.[43−45] This procedure is very efficient, because the potential part of the Hamiltonian matrix is diagonal, which can reduce the memory requirement substantially. The triatomic Hamiltonian in Jacobi coordinates in body fixed frame is given by

$$\hat{H} = -\frac{\hbar^2}{2\mu}\frac{1}{R}\frac{\partial^2}{\partial R^2}R - \frac{\hbar^2}{2\mu}\frac{1}{r}\frac{\partial^2}{\partial r^2}r + \frac{\hat{l}^{\,2}}{2\mu R^2} + \frac{\hat{j}^{\,2}}{2\mu r^2} + V(R,r,\gamma) \quad (1)$$

where the orbital angular momentum is given as

$$\hat{l}^{\,2} = (\hat{J} - \hat{j})^2 = \hat{J}^{\,2} + \hat{j}^{\,2} - 2\hat{J}\cdot\hat{j}$$

Using symmetry-adapted symmetric top eigenfunctions to expand the total wave function, one can get the coupled equations

$$\hat{H}_{\Omega,\Omega} = -\frac{\hbar^2}{2\mu}\frac{1}{R}\frac{\partial^2}{\partial R^2}R - \frac{\hbar^2}{2\mu}\frac{1}{r}\frac{\partial^2}{\partial r^2}r + V(R,r,\gamma) + \left(\frac{1}{2\mu R^2} + \frac{1}{2\mu r^2}\right)\left(-\frac{\hbar^2}{\sin\gamma}\frac{\partial}{\partial\gamma}\sin\gamma\frac{\partial}{\partial\gamma} + \frac{\hbar^2\Omega^2}{\sin^2\gamma}\right) + \frac{\hbar^2}{2\mu R^2}[\,J(J+1) - 2\Omega^2] \quad (2)$$

and

$$\hat{H}_{\Omega,\Omega\pm1} = (1+\delta_{\Omega,m})^{1/2}\frac{\hbar^2}{2\mu R^2}\sqrt{J(J+1)-\Omega(\Omega\pm1)}\left[\pm\frac{\partial}{\partial\gamma}+(\Omega\pm1)\cot\gamma\right] \quad (3)$$

with $m = 0$ for $\hat{H}_{\Omega,\Omega} + 1$ and $m = 1$ for $\hat{H}_{\Omega,\Omega-1}$. Such coupled equations can be represented in DVR:

$$H_{\lambda\Omega}^{\lambda'\Omega'} = -\frac{\hbar^2}{2\mu}\frac{1}{R}\frac{\partial^2}{\partial R^2}R\delta_{\lambda'\lambda}\delta_{\Omega'\Omega} - \frac{\hbar^2}{2\mu}\frac{1}{r}\frac{\partial^2}{\partial r^2}r\delta_{\lambda'\lambda}\delta_{\Omega'\Omega} + V(R,r,\gamma_\lambda^\Omega)\delta_{\Omega'\Omega} + \left(\frac{1}{2\mu R^2}+\frac{1}{2\mu r^2}\right)\sum_j T_{j\lambda}^{\Omega}[j(j+1)\hbar^2]T_{j\lambda'}^{\Omega}\delta_{\Omega'\Omega} + \frac{\hbar^2}{2\mu R^2}[J(J+1)-2\Omega^2]\delta_{\lambda'\lambda}\delta_{\Omega'\Omega} + \sum_j T_{j\lambda}^{\Omega}t_{\Omega,\Omega+1}^{Jj}T_{j\lambda'}^{\Omega+1}\delta_{\Omega'\Omega+1} + \sum_j T_{j\lambda}^{\Omega}t_{\Omega,\Omega-1}^{Jj}T_{j\lambda'}^{\Omega-1}\delta_{\Omega'\Omega-1} \quad (4)$$

with

$$t_{\Omega,\Omega\pm1}^{Jj} = -(1+\delta_{\Omega,m})^{1/2}\frac{\hbar^2}{2\mu R^2}\times\sqrt{J(J+1)-\Omega(\Omega\pm1)}\sqrt{j(j+1)-\Omega(\Omega\pm1)}$$

In eq 4, we have used Ω-dependent DVR for the γ-coordinate, which is obtained by diagonalizing the coordinate operator ($x = \cos\gamma$) matrix,

$$^{\Omega,\gamma}\Delta_{jj'} = \int_{-1}^{1}\Theta_j^\Omega(\gamma)x\Theta_{j'}^\Omega(\gamma)\,dx$$

Here, $\Theta_j^\Omega(\gamma)$ is the associated Legendre polynomial. In the direct diagonalization scheme, the DVR points and the transformation matrix are simply the eigenvalues and the eigenvector matrix of the coordinate operator matrix. For R and r coordinates, we have used potential-optimized DVR.[46] The details of the DVRs will be given in section 3.

2.2. Propagation. In the Lanczos iteration, we choose a normalized, randomly generated initial vector, $v_1 \neq 0$, and set $\beta_1 = 0$ and $v_0 = 0$. We then use the basic Lanczos algorithm for complex-symmetric matrices,[47]

$$\beta_{k+1}v_{k+1} = \hat{H}'v_k - \alpha_k v_k - \beta_k v_{k-1} \quad (5)$$

to project the non-Hermitian absorbing potential augmented Hamiltonian into a Krylov subspace. The $M \times M$ tridiagonal representation of the Hamiltonian, T_M, has diagonal elements $\alpha_k = (v_k|\hat{H}'|v_k)$, and subdiagonal elements $\beta_k = (v_{k-1}|\hat{H}'|v_k)$. Note that a complex-symmetric inner product is used (i.e., bra vectors are not complex conjugated). The two vectors, $\{\alpha\}$ and $\{\beta\}$, are stored in Lanczos iterations for later analysis to extract physical information such as bound state or resonance quantities.

Although conceptionally simple, the propagation is the most time-consuming part of the calculation. We use modified perturbation iteration (MPI) to perform parallel computation for the matrix-vector multiplications. For even spectroscopic symmetry, the four-dimensional (4-D) matrix-vector multiplication looks like

$$\begin{pmatrix} H_{00} & H_{01} & 0 & 0 \\ H_{10} & H_{11} & H_{12} & 0 \\ 0 & H_{21} & H_{22} & \ddots \\ 0 & 0 & \ddots & \ddots \end{pmatrix}\begin{pmatrix} \psi_{\Omega=0} \\ \psi_{\Omega=1} \\ \psi_{\Omega=2} \\ \vdots \end{pmatrix} = \begin{pmatrix} \phi_{\Omega=0} \\ \phi_{\Omega=1} \\ \phi_{\Omega=2} \\ \vdots \end{pmatrix} \quad (6)$$

with $\phi_\Omega = H_{\Omega,\Omega-1}\psi_{\Omega-1} + H_{\Omega,\Omega}\psi_\Omega + H_{\Omega,\Omega+1}\psi_{\Omega+1}$. For odd spectroscopic symmetry, the Hamiltonian matrix is the same, except $\Omega = 1, 2, ..., J$. The spectroscopic symmetry parity is defined as $(-1)^{J+p}$, with p being the parity of the wave function under inversion of the space fixed nuclear coordinates. We adopt a natural way to distribute the problem, with respect to the Ω block, which will make the calculations of $\{\alpha\}$ and $\{\beta\}$ much easier and the modifications of our code as little as possible for parallel computing. We assign one processor as the master processor (ID = 0), which is used to write $\{\alpha\}$ and $\{\beta\}$, and assign all other processors as working processors, which are used to perform the matrix-vector multiplications for different Ω components. Our implementation has the flexibility that any number of CPUs ($2 \leq n \leq J + 2$) can be used in our Sun cluster machine. The details of our parallelization method have been given in previous work (see, e.g., ref 41). We note that the related parallel model of Goldfield et al. has been used in reactive scattering calculations.[48−50]

2.3. Final Analysis. After the tridiagonal matrix T_M is generated, we calculate the eigenvalues of T_M, using the standard QL algorithm. As mentioned in the Introduction, the complications are the ghosting eigenvalues, which must be removed, and we have devised an algorithm to identify all the true converged eigenvalues from single Lanczos iterations, which we believe has significant advantages of previously established methods (e.g., refs 3, 8, 9). We summarize the algorithm as follows, and the technical details will be given in section 3.

(i) Calculate the error norm for each eigenvalue E_j generated from T_M, through

$$\sigma(E_j) = ||(T_M - E_j)\phi(E_j)|| \quad (7)$$

Clearly, true eigenvalues (or their copies) should have small error norms and, therefore, can be distinguished from any unconverged/spurious eigenvalues. Thus, if the error norm of the eigenvalue is larger than a prescribed value (for example, $\delta = 10^{-4}$), the eigenvalue is regarded as unconverged or spurious and will be removed. The Lanczos subspace eigenvector $\phi(E_j)$ in eq 7 can be regenerated inexpensively for each complex eigenenergy, through a backward substitution recursion:

For all j =1, 2, ..., M, generate $\phi(E_j)$ by solving the subspace Schrödinger equation:

$$(E_j - T_M)|\phi(E_j)\rangle = 0 \quad (8)$$

(a) Choose ϕ_M, the Mth element of $\phi(E_j)$, to be arbitrary (but nonzero; this is usually set to be $\phi_M = 1$), and calculate

$$\phi_{M-1} = \frac{1}{\beta_M}(E_j\phi_M - \alpha_M\phi_M) \quad (9)$$

(b) For $k = M - 1, M - 2, ..., 2$, update the scalar ϕ_{k-1}:

$$\beta_k\phi_{k-1} = E_j\phi_k - \alpha_k\phi_k - \beta_{k+1}\phi_{k+1} \quad (10)$$

(c) There is a constant difference between the subspace wave function generated through this way and the true subspace wave function. Normalize the generated subspace wave function to determine the constant.

(ii) After step (i), there will still be multiple eigenvalues clustered about the true eigenvalues at the low- or high-energy component, which are indeed very close to the true eigenvalue. We call them copies of the true eigenvalues. Remove the copies, replacing each group of multiplet eigenvalues lying within the range Δ (where Δ is very small, e.g., 10^{-6}) by the single eigenvalue *with the smallest error norm*. In the Lanczos method, the emergence of multiplets of an eigenvalue is an indication of the convergence of the eigenvalue.

The efficiency of this identification algorithm relies on the very efficient three-term backward recursion procedure to generate the subspace wave function, because the overhead for calculating the error norms is minor, using the three-term recursion. Also, the new algorithm does not require the diagonalization of the tridiagonal matrix T_M twice, as is required in most applications, to extract all eigenvalues using the Cullum and Willoughby (CW) method.[3] In the CW method, a submatrix T', which is derived by deleting the first row and first column of the tridiagonal Lanczos matrix T_M, is diagonalized. The common eigenvalues of the two matrices are identified as spurious and discarded. The present method is competitive with, e.g., a bisection approach to determining eigenvalues of the tridiagonal but, in contrast, must be performed only once. Here, we note that if the chosen M is not large enough to converge the required eigenvalues, we can always restart the Lanczos iterations, as long as we keep the latest two Lanczos vectors. Finally, we must mention that this method does not enable degenerate eigenvalues to be resolved. For that purpose, please refer to Paige's method.[20]

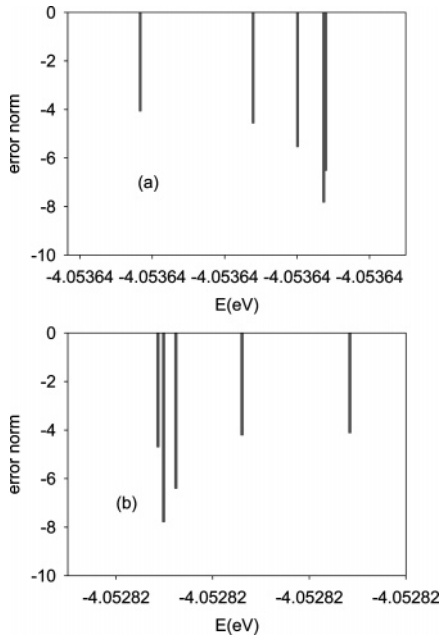

Figure 2. (a) Plot of the logarithmic error norms for the copies of the first eigenvalue at $E = -4.053640$ eV from the $J = 30$ and even symmetry calculations. All the clustering eigenvalues with error norms of $>10^{-4}$ are removed. From the group of the copies, the fourth one with the smallest error norm will be picked up as the true eigenvalue. (b) Plot of the logarithmic error norms for the copies of the second eigenvalue at $E = -4.052824$ eV from the $J = 30$ and even symmetry calculations. All the clustering eigenvalues with error norms of $>10^{-4}$ are removed. From the copies, the second one with the smallest error norm will be picked up as the true eigenvalue.

3. Results

3.1. Calculational Details. The triatomic Hamiltonian matrix was set up in terms of reactant Jacobi coordinates, and the improved version of the ab initio PES recently developed by Nanbu et al.[40] was applied. In the new version, 1761 points have been added in the vicinity of the equilibrium to refine the first-generation PES. For the two radial coordinates, a potential-optimized DVR[46] (PODVR) was utilized to reduce the size of the Hamiltonian matrix. For the R-coordinate, we have used $N_R = 130$ PODVR points, which were contracted from 360 evenly spaced primitive sinc DVR points,[51] spanning the range from $2.0a_0$ to $12.0a_0$ with the one-dimensional reference potential, $V(R,r_e,\theta_e)$. Similarly, for the r-coordinate, $N_r = 80$ PODVR points were obtained from 245 primary DVR points, spanning the range from $1.0a_0$ to $6.0a_0$ using the reference potential, $V(R_e,r,\theta_e)$. For the γ-variable, Ω-dependent DVR functions, which are defined by correspondingly associated Gauss−Jacobi quadrature points, were used. The spectroscopic symmetry that originated from the Wigner D-functions has also been considered. The resulting direct product basis set was further contracted by discarding those points whose potential energies were higher than the cut-off energy, $V_{cutoff} = 0.48$ eV (here, the zero energy point is referred to as the dissociation limit of $O(^1D) + DCl$ channel), resulting in the final basis size of $\sim 389\,700 \times (J + 1)$ for even spectroscopic symmetry and $\sim 389\,700 \times J$ for odd spectroscopic symmetry. In our calculations, the Lanczos propagations and final analysis are completely separated. Although parallel computations are used only in the propagation step, the final analyses are performed using conventional nonparallel architectures. Eight CPUs have been used for both even and odd spectroscopic symmetries for the $J = 30$ case.

3.2. Test of the Algorithm. Before presenting the results, we check the algorithm of identifying all the true converged eigenvalues for the $J = 30$ and even spectroscopic symmetry case. The Hamiltonian matrix size in the primary representation is $12\,080\,700 \times 12\,080\,700$, which is the largest among all our previous calculations. The Lanczos iteration number used is $M = 150\,000$. In Figure 1, we show the logarithmic error norms for the DOCl clustering eigenvalues around the first two lowest eigenvalues at $E = -4.053640$ eV and $E = -4.052824$ eV. Here, the ro-vibrational state energy was relative to the $O(^1D) + DCl$ dissociation limit, which is called the zero energy point. The eigenvalues are computed through direct diagonalization of the tridiagonal matrix, which consist of true eigenvalues and spurious eigenvalues. The latter are produced by the loss of orthogonality during the Lanczos iteration. From this figure, we can see that hundreds of spurious eigenvalues surround the two true eigenvalues, which have the smallest error norms. Most other eigenvalues have error norms that are larger than our prescribed small value ($\delta = 10^{-4}$) and therefore can be regarded as spurious and can be removed through our algorithm. Only four multiplet eigenvalues close to the first true eigenvalue (see Figure 2a) and four multiplet eigenvalues close to the second true eigenvalue (see Figure 2b) have error norms smaller than the prescribed small value δ and can be regarded as the copies of the two true eigenvalues and remain. Because the group of eigenvalues are very close and are well-separated from the remaining eigenvalues, we can easily identify the one with the smallest error norm as the true eigenvalue. Indeed, in terms of resonance energy, each of these copies is well-converged, and in some algorithms, any copy can be picked up as the true eigenvalue, but the most accurate eigenvalue should correspond to the one with the smallest error norm. This is particularly true for resonance width (imaginary part of the eigenvalue), which exhibits some noticeable differences among the copies. The

TABLE 1: Comparison of the HOCl Vibrational Energies of the First 14 Bound States at $J = 0$ for the Old Version and the Improved Version of the Ab Initio Potential Energy Surfaces (PESs)

		Vibrational Energy[a] (cm^{-1})			
n	(ν_1,ν_2,ν_3)[a]	new PES	old PES	Bowman et al.[25]	experiment
1	0,0,0	0.00	0.00	0.000	
2	0,0,1	724.97	650.58	724.336	724.36
3	0,1,0	1245.10	1261.97	1238.617	1238.62
4	0,0,2	1442.30	1309.21	1444.107	1438.68
5	0,1,1	1967.40	1926.92	1953.748	
6	0,0,3	2161.35	1963.22	2154.028	
7	0,2,0	2458.67	2522.28	2456.363	2461.21
8	0,1,2	2684.90	2592.00	2663.255	
9	0,0,4	2869.56	2615.53	2852.172	
10	0,2,1	3178.06	3185.19	3163.826	
11	0,1,3	3404.64	3245.26	3362.256	
12	0,0,5	3568.77	3268.65	3537.056	
13	1,0,0	3615.22	3599.72	3609.972	3609.48
14	0,3,0	3670.61	3792.41	3670.391	3668.44

[a] Quantum numbers (ν_1,ν_2,ν_3) are used to label the energy levels. [b] Bowman et al.'s results and the available experimental data are also included. See text for more details.

above algorithm is very sharp and sensitive in identifying the true eigenvalues, because of the Green function property implied in eq 8. Thus, the new algorithm offers a simple and accurate alternative approach to identification of the true eigenvalues, because it picks up the one with the smallest error norms from the copies. This is particularly useful for accurately calculating resonance widths.

3.3. Ro-vibrational State Calculations. We have used the Lanczos method previously summarized to compute all the bound states and low-lying resonances for the $J = 0$ case, and the low-lying rovibrational bound state manifold of the DOCl at $J = 30$ for both spectroscopic symmetries. To facilitate the comparisons with previous reported calculations and with the experimental results, in the following tables, the calculated energies are shifted by 4.106248 eV, such that the zero energy point is called the $J = 0$ vibrational ground-state energy, and the energy units are changed to cm^{-1}. First, we test the performance of the new version of the ab initio PES for the HOCl $J = 0$ case. Two thousand Lanczos iterations are sufficient to converge the lowest bound states, and in Table 1, we have listed the 14 lowest bound state energies from the $J = 0$ calculations for comparison. In this table, the second column contains the spectroscopic assignments of the states, with ν_1, ν_2, and ν_3 being the number of quanta in the OH stretching, HOCl bending, and OCl stretching local modes, respectively. The third column contains the results calculated with the present quantum Lanczos method on the new PES, whereas the fourth column contains the results from previous Lanczos subspace filter diagonalization method on the old ab initio PES.[41] The fifth column provides the reported results from Bowman et al.,[34] and the last column gives the available spectroscopic data.[30,52−55] Inspection of the table indicates that the new version of the pure ab initio PES generates the vibrational energies, which are in much better agreement with the available experimental data and with the early results of Bowman et al. It is important to stress again at this point that the PES of Nanbu et al.[40] that we use in this paper is a genuine ab initio surface, without being scaled and/or inverted to reproduce the 22 available experimental vibrational bound state energies, as was previously done for the other two high-quality ab initio PESs.[38,39] Another technical point is that spline interpolation of potential energies at grid points has been applied in this PES, whereas in the other two PESs, fitted analytical expansions have been used. The new global ab initio PES gives a better representation about the minimum, because it has been developed and tested initially with a view to reactive scattering calculations.

TABLE 2: DOCl Vibrational Energies of the Lowest 10 Bound States at $J = 0$, Calculated Using the Improved Version of the Ab Initio Potential Energy Surface (PES)[a]

		Vibrational Energy (cm^{-1})	
n	(ν_1,ν_2,ν_3)	calculated	experimental
1	(0,0,0)	0.00	0.0
2	(0,0,1)	722.588	723.3
3	(0,1,0)	916.213	909.6
4	(0,0,2)	1436.187	
5	(0,1,1)	1639.235	
6	(0,2,0)	1808.916	
7	(0,0,3)	2150.011	
8	(0,1,2)	2358.013	
9	(0,2,1)	2532.055	
10	(1,0,0)	2669.201	2665.6

[a] Other symbols are the same as those used in Table 1.

In Table 2, we have elected to present the 10 lowest bound state energies from DOCl $J = 0$ calculations on the new PES. To generate all the bound state spectra and the low-lying resonance spectra, the number of Lanczos iterations used is $M = 150\,000$. In this table, the second column again contains the spectroscopic assignments of the states, with ν_1, ν_2, and ν_3 being the number of quanta in the OD stretching, DOCl bending, and OCl stretching local modes, respectively. The third column contains the results calculated with the present Lanczos method, whereas the fourth column provides the available spectroscopic data.[21,22] Inspection of the table indicates that the three fundamentals are reproduced reasonably well using the new PES, which gives us the confidence to compute the full spectra for the $J = 0$ case (see below discussion regarding the density of states (DOS)). For the $J = 30$ case, 150 000 Lanczos iterations also are used to generate the lower portion of the ro-vibrational bound states for both spectroscopic symmetries. The spectrum for the $J = 30$ case is much denser than the $J = 0$ case and converges more slowly, and, as such, the exact quantum calculations (including Coriolis coupling terms) are still very challenging, due, in part, to the ever-increasing size of the basis set; therefore, we focus on the lower portion of the spectrum in this paper. For instance, three months of wall time are required to converge the reported bound state energies for the $J = 30$ and even symmetry case, using eight CPUs (four nodes) of an Opteron dual-processor 2.2 GHz grid. Without the combination of parallel computing with the more-advanced methodology, it would be exceedingly difficult, of not prohibitive, to perform these benchmark test calculations. In Table 3, we select the 19 ro-vibrational bound states within the (1,0,0) manifold to contrast with the available experimental data[21,22] and with the approximate results from adiabatic rotation.[56] In this table, the calculated bound states can be assigned in terms of the three fundamentals ν_1, ν_2, and ν_3 and in terms of J, K_a, and K_c. Here, quantum numbers K_a and K_c are used to label the energy levels, using the rigid rotor approximation, because DOCl is almost a symmetric top (K_a is indeed the same as Ω). Comparison of the observed high-resolution ro-vibrational energy levels and the computed ones indicates that the differences for all the levels are <5 cm^{-1}. Such differences are mainly due to the level of accuracy in the PES calculations, not the ro-vibrational dynamics calculations, because the origin of the vibrational band (1,0,0) has already had a difference of 3.6 cm^{-1} between the experiment and the calculation (see Table 2). The results indicate that, although the purely ab initio PESs/exact quantum dynamics calculations have not yet reached spectroscopic levels of

TABLE 3: Comparison of Experimental and Calculated Results for Selected DOCl Ro-vibrational State Energies for the $J = 30$ Case

	Ro-vibrational State Energy (cm^{-1})					
n	exact	AR	experimental	(J,K_a,K_c)	(ν_1,ν_2,ν_3)	symmetry
1	3100.14	3102.29	3096.8861	(30,0,30)	(1,0,0)	even
2	3104.89	3112.57	3103.1051	(30,1,30)	(1,0,0)	even
3	3139.87	3143.41	3138.8417	(30,2,29)	(1,0,0)	even
4	3187.37	3194.80	3190.3545	(30,3,28)	(1,0,0)	even
5	3263.19	3266.75	3261.8675	(30,4,27)	(1,0,0)	even
6	3358.46	3359.25	3353.6688	(30,5,26)	(1,0,0)	even
7	3466.33	3472.31	3465.6222	(30,6,25)	(1,0,0)	even
8	3599.97	3605.93	3597.5640	(30,7,24)	(1,0,0)	even
9	3755.51	3760.11		(30,8,23)	(1,0,0)	even
10	3929.19	3934.84		(30,9,22)	(1,0,0)	even
11	3112.29	3112.57	3112.88	(30,1,29)	(1,0,0)	odd
12	3142.07	3143.41	3139.9768	(30,2,28)	(1,0,0)	odd
13	3187.40	3194.80	3190.3886	(30,3,27)	(1,0,0)	odd
14	3264.78	3266.75		(30,4,26)	(1,0,0)	odd
15	3357.59	3359.25		(30,5,25)	(1,0,0)	odd
16	3467.18	3472.31		(30,6,24)	(1,0,0)	odd
17	3599.20	3605.93		(30,7,23)	(1,0,0)	odd
18	3756.52	3760.11		(30,8,22)	(1,0,0)	odd
19	3927.92	3934.84		(30,9,21)	(1,0,0)	odd

[a] See text for more details.

accuracy for the calculation of small molecules, we are getting closer to our goals. Of course, the experimental measurements are not always easy, because of the weak nature of some transitions and the lack of some infrared transitions of sufficient strength. In this respect, theoretical predictions are complementary to the experimental measurements.

To test the adiabatic rotation approximations for high J values, we have performed the approximation calculations using Bowman et al.'s adiabatic rotation method[56] for the low bound state energies. The rotation constants A, B, and C used in this work are taken from experimental results,[21,22] e.g., (10.74401, 0.47632516, 0.45505155) for the (1,0,0) band (given in units of cm^{-1}). Comparison of the quantum and AR results in the table shows that, for DOCl systems, the AR approximation still predicts good results, even for the $J = 30$ case. These results indicate that the mixing of different Ω components of the wave function for $J > 0$ is not apparent, and AR results are indeed very close to the exact quantum results, at least for the low-energy part. In other words, the quantum number Ω is still generally a good quantum number. This can be seen through a comparison of the energy levels with the same K_a but from different spectroscopic symmetries. If the calculated energies from even and odd symmetries are almost the same for the same Ω component, then Ω is a good quantum number. This is because there exists near degeneracy for the same Ω components from both symmetries. By such comparison of the corresponding energy levels, we can see that, for the DOCl system, there does exist near degeneracy for the same Ω components from both symmetries, indicating that Ω is indeed a good quantum number. Therefore, for the DOCl system, the much-simpler adiabatic rotation approximations should be accurate, which will save quite a lot of computational time. We also note whenever the energy levels become close (e.g., the first two energy levels in the band), the mixing of different Ω components is more serious, and the differences in the corresponding energy levels become relatively large.

Having calculated the ro-vibrational states, it is straightforward to compute the J-resolved DOS. The DOS is a very important quantity in various statistical theories of unimolecular reaction dynamics. To calculate the DOS, we apply the method of direct counting of both bound and resonance states in the bin. In Figure 3, we report the DOCl quantum DOS in both the bound and low-lying dissociation resonance regimes for the $J = 0$ case. Here, the zero energy point is referred to the $O(^1D) + HCl$ dissociation limit, and the first $Cl(^2P) + OH$ dissociation limit is observed at $-15486\ cm^{-1}$. The bin length used for direct counting is 1 kcal/mol, and the units for the quantum density of states $\rho(E)$ are states/cm^{-1}. From Figure 3, we can see that $\rho(E)$ fluctuates, in particular at the higher-energy part. At the $Cl(^2P) + OH$ dissociation limit, the calculated DOS is $\sim$0.24 states/cm^{-1}, which is slightly higher than the value of 0.2 states/cm^{-1} that has been previously reported for HOCl at its first threshold.[34] In Figure 4, we report $\rho(E)$ for the DOCl system at $J = 30$. In this plot, the ro-vibrational states from both even and odd spectroscopy symmetry have been included. Comparison with the results in Figure 3 shows that the DOS at $J = 30$ is much higher than that at $J = 0$.

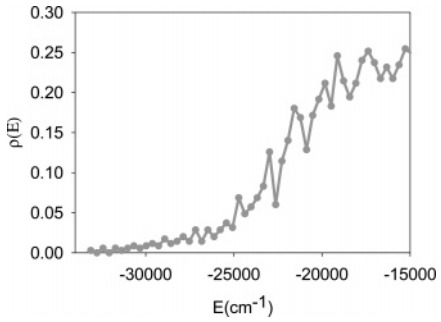

Figure 3. Quantum density of states ($\rho(E)$) for the DOCl $J = 0$ case, which are calculated through direct counting of both the bound and resonance states in the bin. Bin length = 1 kcal/mol. The units for $\rho(E)$ are states/cm^{-1}, and the units for energy are cm^{-1}. Here, the zero energy point is considered to be the $O(^1D) + HCl$ dissociation limit, and the first dissociation limit for $Cl(^2P) + OH$ is observed at $-15\,486$ cm^{-1}.

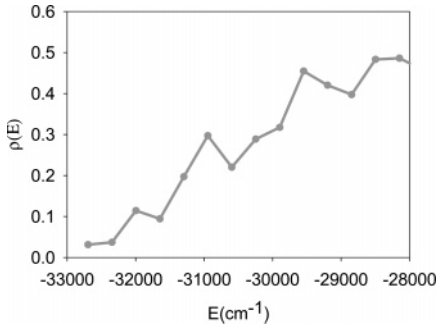

Figure 4. Quantum density of states ($\rho(E)$) for the DOCl $J = 30$ case; ro-vibrational states from both even and odd spectroscopy symmetry have been included. Other symbols are the same as those given in Figure 3.

4. Conclusions

In this paper, an improved Lanczos method has been combined with a parallel computing strategy to calculate the ro-vibrational states and corresponding density of states (DOS) for the DOCl system at a total angular momentum of $J = 0$ and $J = 30$, using an augmented version of the ab initio potential energy surface (PES) of Nanbu et al.[40] An algorithm that is based on error norm analysis to identify all the true eigenvalues has been proposed and tested on the DOCl system. For the $J = 0$ case, all the vibrational states and the low-lying resonances have been extracted from a single Lanczos iteration, and for the $J = 30$ case, the dense spectra of the low bound states have been computed. The algorithm proves to be accurate and more efficient, even for the very large primary matrix size of more

than 10^6 for the $J = 30$ case. For ro-vibrational spectroscopy calculations, the comparison between experimental results and the exact quantum mechanical calculations indicates that the new version of the pure ab initio PES is much better than the previous counterpart in regard to predicting vibrational band origins and the ro-vibrational energy levels. The widely used approximate adiabatic rotation method has been tested for the selected states at $J = 30$, and the results indicate that the adiabatic rotation approximation performs well for the DOCl system. Through analysis of the energy levels with the same K_a but from different spectroscopic symmetries, we can see that Ω is generally a good quantum number for the low-energy part of the bound state manifold, which implies that Coriolis coupling does not seem to be as important as it is in other deep well systems, such as in HO_2. Clearly, the methods of this work would facilitate extension for the investigation of resonances in HOCl/DOCl systems for nonzero total angular momentum, which is still a very challenging proposition, even for modest values of J.

Acknowledgment. We are grateful to the Australian Research Council and The University of Queensland for supporting this work. Generous grants of high-performance computer time are acknowledged from The University of Queensland (namely, the Computational Molecular Science cluster computing facility) and the Australian Partnership for Advanced Computing (APAC) National Facility.

References and Notes

(1) Light, J. C.; Hamilton, I. P.; Lill, J. V. *J. Chem. Phys.* **1985**, *82*, 1400.
(2) Lanczos, C. *J. Res. Natl. Bur. Stand.* **1950**, *45*, 255.
(3) Cullum, J. K.; Willoughby, R. A. *Lanczos Algorithms for Large Symmetric Eigenvalue Computations*; Birkhauser: Boston, 1985; Vol. 1.
(4) Park, T. J.; Light, J. C. *J. Chem. Phys.* **1986**, *85*, 5870.
(5) Smith, S. C.; Jeffrey, S. J. *J. Chem. Phys.* **1996**, *105*, 4055.
(6) Jeffrey, S. J.; Smith, S. C.; Clary, D. C. *Chem. Phys. Lett.* **1997**, *273*, 55.
(7) Jeffrey, S. J.; Smith, S. C. *Chem. Phys. Lett.* **1997**, *278*, 345.
(8) Yu, H. G.; Smith, S. C. *Ber. Bunsen. Phys. Chem.* **1997**, *101*, 400.
(9) Yu, H. G.; Smith, S. C. *J. Comput. Phys.* **1998**, *143*, 484.
(10) Yu, H. G.; Smith, S. C. *Chem. Phys. Lett.* **1998**, *283*, 69.
(11) Smith, S. C.; Yu, H. G.; Leforestier, C.; Rayez, J. C. *Phys. Chem. Chem. Phys.* **1999**, *1*, 1311.
(12) Zhang, H.; Smith, S. C. *Phys. Chem. Chem. Phys.* **2001**, *3*, 2282.
(13) Zhang, H.; Smith, S. C. *Chem. Phys. Lett.* **2001**, *347*, 211.
(14) Zhang, H.; Smith, S. C. *J. Chem. Phys* **2001**, *115*, 5751.
(15) Zhang, H.; Smith, S. C. *J. Chem. Phys.* **2002**, *116*, 2354.
(16) Rasmussen, A. J.; Jeffrey, S. J.; Smith, S. C. *Chem. Phys. Lett.* **2001**, *336*, 149.
(17) Zhang, H.; Smith, S. C. *J. Theor. Comput. Chem.* **2003**, *2*, 563.
(18) Zhang, H.; Smith, S. C. *J. Chem. Phys.* **2004**, *120*, 1161.
(19) Reignier, D.; Smith, S. C. *Chem. Phys. Lett.* **2002**, *366*, 390.
(20) Paige, C. C. *J. Inst. Math. Appl.* **1972**, *10*, 373.
(21) Deeley, C. M. *J. Mol. Spectrosc.* **1987**, *122*, 481.
(22) Zheng, J.-J.; Ulenikov, O. N.; Bekhtereva, E. S.; Ding, Y.; He, S.-G.; Hu, S.-M.; Wang, X.-H.; Zhu, Q.-S. *J. Mol. Spectrosc.* **2001**, *209*, 105.
(23) Truhlar, D. G. *Comput. Phys. Commun.* **1994**, *84*, 78.
(24) Bacic, Z.; Light, J. C. *Annu. Rev. Phys. Chem.* **1989**, *40*, 469.
(25) Bowman, J. M.; Gazdy, B. *J. Chem. Phys.* **1991**, *94*, 454.
(26) Jensen, P.; Buenker, R. J.; Gu, J. P.; Osmann, G.; Bunker, P. R. *Can. J. Phys.* **2001**, *79*, 641.
(27) Osmann, G.; Bunker, P. R.; Jensen, P.; Buenker, R. J.; Gu, J. P.; Hirsch, G. *J. Mol. Spectrosc.* **1999**, *197*, 262.
(28) Chance, K. V.; Johnson, D. G.; Traub, W. A. *J. Geophys. Res.* **1989**, *94*, 11059.
(29) Carlotti, M.; Lonardo, G. D.; Fusina, L.; Trombetti, A.; Carli, B. *J. Mol. Spectrosc.* **1990**, *141*, 29.
(30) Flaud, J.-M.; Birk, M.; Wagner, G.; Orphal, J.; Lafferty, S. K. J. *J. Mol. Spectrosc.* **1998**, *191*, 362.
(31) Chu, T. S.; Zhang, Y.; Han, K. L. *Int. Rev. Phys. Chem.* **2006**, *25*, 201.
(32) Lin, S. Y.; Han, K. L.; Zhang, J. Z. H. *Phys. Chem. Chem. Phys.* **2000**, *2*, 2529.
(33) Lin, S. Y.; Han, K. L.; Zhang, J. Z. H. *Chem. Phys. Lett.* **2000**, *324*, 122.
(34) Skokov, S.; Qi, J.; Bowman, J. M.; Yang, C.-Y.; Gray, S. K.; Peterson, K. A.; Mandelshtam, V. A. *J. Chem. Phys.* **1998**, *109*, 10273.
(35) Mussa, H. Y.; Tennyson, J. *Chem. Phys. Lett.* **2002**, *366*, 449.
(36) Yang, H.; Han, K.-L.; Nanbu, S.; Nakamura, H.; Balint-Kurti, G. G.; Zhang, H.; Smith, S. C.; Hankela, M. *J. Chem. Phys.* **2007**, *127*, in press.
(37) Skokov, S.; Peterson, K. A.; Bowman, J. M. *J. Chem. Phys.* **1998**, *109*, 2662.
(38) Skokov, S.; Peterson, K. A.; Bowman, J. M. *Chem. Phys. Lett.* **1999**, *312*, 494.
(39) Weib, J.; Hauschildt, J.; Grebenshchikov, S. Y.; Duren, R.; Schinke, R.; Koput, J.; Stamatiadis, S.; Farantos, S. C. *J. Chem. Phys.* **2000**, *112*, 77.
(40) Nanbu, S.; Aoyagi, M.; Kamisaka, H.; Nakamura, H.; Bian, W.; Tanaka, K. *J. Theor. Comput. Chem.* **2002**, *1*, 263.
(41) Zhang, H.; Smith, S. C.; Nanbu, S.; Nakamura, H. *J. Phys. Chem. A* **2006**, *110*, 5468.
(42) Bowman, J. M. *Chem. Phys. Lett.* **1993**, *217*, 36.
(43) Choi, S. E.; Light, J. C. *J. Chem. Phys.* **1990**, *92*, 2129.
(44) Leforestier, C. *J. Chem. Phys.* **1991**, *94*, 6388.
(45) Auerbach, S. M.; Miller, W. H. *J. Chem. Phys.* **1994**, *100*, 1103.
(46) Echave, J.; Clary, D. *Chem. Phys. Lett.* **1992**, *190*, 225.
(47) Moro, G.; Freed, J. H. *J. Chem. Phys.* **1981**, *74*, 3757.
(48) Meijer, A.; Goldfield, E. M. *J. Chem. Phys.* **1998**, *108*, 5404.
(49) Meijer, A.; Goldfield, E. M. *J. Chem. Phys.* **1999**, *110*, 870.
(50) Goldfield, E. M.; Meijer, A. J. H. M. *J. Chem. Phys.* **2000**, *113*, 11055.
(51) Colbert, D. T.; Miller, W. H. *J. Chem. Phys.* **1992**, *96*, 1982.
(52) Lafferty, W. J.; Olson, W. B. *J. Mol. Spectrosc.* **1986**, *120*, 359.
(53) Deeley, C. M.; Mills, I. M. *J. Mol. Spectrosc.* **1985**, *114*, 368.
(54) Wells, J. S.; Sams, R. L.; Lafferty, W. J. *J. Mol. Spectrosc.* **1979**, *77*, 349.
(55) Azzolini, C.; Cavazza, F.; Crovetti, G.; Lonardo, G. D.; Frulla, R.; Escribano, R.; Fusina, L. *J. Mol. Spectrosc.* **1994**, *168*, 494.
(56) Qi, J.; Bowman, J. M. *J. Chem. Phys.* **1996**, *105*, 9884.